ACS OMEGA

http://pubs.acs.org/journal/acsodf

Article

# Phonon Hydrodynamic Transport: Observation of Thermal Wave-Like Flow and Second Sound Propagation in Graphene at 100 K

Houssem Rezgui*

Cite This: *ACS Omega* 2023, 8, 23964−23974

Read Online

ACCESS | Metrics & More | Article Recommendations | Supporting Information

**ABSTRACT:** Several experimental and theoretical investigations confirm the failure of the classical Fourier's law in low-dimensional systems and ultrafast thermal transport. Hydrodynamic heat transport has been recently considered as a promising avenue to thermal management and phonon engineering in graphitic materials. Non-Fourier features are therefore required to describe and distinguish the hydrodynamic regime from other heat transport regimes. In this work, we provide an efficient framework for the identification of hydrodynamic heat transport and second sound propagation in graphene at 80 and 100 K. We solve both the dual-phase-lag model and the Maxwell−Cattaneo−Vernotte equation based on the finite element method with ab initio data as inputs. We emphasize on the detection of thermal wave-like behavior using macroscopic quantities including the Knudsen number and second sound velocity beyond Fourier's law. We present a clear observation of the crossover phenomena from the wave-like regime to diffusive heat transport predicted in terms of mesoscopic equations. This present formalism will contribute to a clear and deeper understanding of hydrodynamic heat transport in condensed systems for future experimental detection of second sound propagation above 80 K.

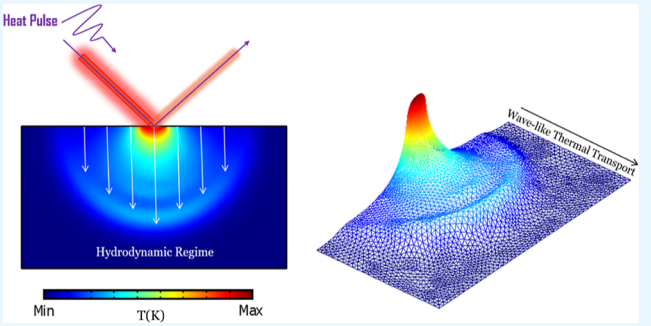


## 1. INTRODUCTION

Due to the rapid progress in semiconductor manufacturing, thermal management becomes a key point for controlling heat transport in nanoelectronic devices including diodes[1,2] and nanotransistors.[3,4] Since 2015, processors contain 10 billion MOSFETs with the characteristic channel length below 20 nm.[5] The aggressive scaling down of nanoelectronic devices leads to reduced thermal conductivity and therefore causes a hot spot temperature within the ultrashort channel transistor.[6,7] During recent years, the electronic device community has focused on two-dimensional (2D) materials to avoid the undesirable leakage current and self-heating effects in emerging nano-devices.[5] However, modeling of hot spot temperature is under debate due to the complexity of the phonon transport at the nanoscale, which increases the effective thermal resistance of the device. To solve this critical issue, several experimental and theoretical studies were developed to investigate the localized hot spot temperature and the self-heating process by mapping the temperature distribution within the device.[8−10] Although many research efforts have been proposed, there is still a lack of a deeper understanding of ultrafast thermal transport in 2D materials.

In general, heat propagation in solid materials is characterized by phonon interactions and scattering mechanisms. In many situations, the phonon flow cannot be predicted by a single regime; however, three different regimes can coexist: (1) ballistic regime (external boundary scattering), (2) hydrodynamic regime (the total momentum is conserved during phonon−phonon scattering), and (3) diffusive regime (momentum destruction due to resistive scattering).[11] In comparison to the diffusive heat transport, the hydrodynamic transport coincides with the wave-like propagation invoked by a heat pulse. The wave-like heat transport is confirmed by observing the temperature oscillation behavior in ballistic,[12] quasiballistic,[13] and hydrodynamic regimes.[14−17] In the hydrodynamic regime, the classical Fourier's law breakdown cannot explain the thermal wave propagation when normal ($N$) scattering dominates the phonon flow. In this regime, the heat propagation is treated based on the drift motion of phonon flow similar to pressure gradient, leading to second sound propagation.[14] Here, the heat transport behavior should be described beyond Fourier's law with a novel and challenging physical picture. In the ballistic regime, the heat pulse propagates close to the group velocity of longitudinal acoustic and transversal acoustic modes around $T$ = 30 K.[12] For the quasiballistic regime, the heat pulse propagates faster than the second sound velocity but slower than

**Received:** April 14, 2023
**Accepted:** June 9, 2023
**Published:** June 20, 2023





https://doi.org/10.1021/acsomega.3c02558
*ACS Omega* 2023, 8, 23964−23974

the ballistic pulse. In the diffusive regime, the resistive ($R$) scattering processes destroy the phonon momentum, and the heat pulse cannot propagate as a damped wave. In contrast, there is still a lack of illustrative methods to distinguish both quasiballistic and hydrodynamic regimes. The wave-like behavior is not sufficient for the description of the picture of transient phonon hydrodynamic transport at temperatures around 80 and 100 K.

The transient non-Fourier heat transfer is a promising feature for the description of ultrafast thermal transport and second sound propagation in 2D materials.[18] Nowadays, non-Fourier behavior provides a good agreement with the experimental data of the transient thermal grating,[16,19] lattice Boltzmann method,[20] and ab initio (first-principles) calculations.[18,21] The second sound transport appears in a hydrodynamic regime and can be probed by non-Fourier transient phonon flow. In conventional solids, the second sound propagation remains an exotic phenomenon that occurs in the transition between ballistic and hydrodynamic regimes at extremely low temperatures (cryogenic condensed system). Hydrodynamic heat transport has been observed in solid helium below 1 K,[22] bismuth (around 3.5 K),[23] and within the temperature range 10 < $T$ < 25 K for NaF.[24] Recent observations of hydrodynamic phonon transport have confirmed that the hydrodynamic regime can occur even at the highest temperature in graphite above 100 K.[25] The hydrodynamic phenomena emerge when the applied heat pulse propagates as a damped wave caused by $N$-scattering. Quite remarkably, in graphitic materials (graphene,[15] graphane,[15] and graphite[25]), $N$-scattering events that conserve the momentum still dominate even at the highest temperature, and it is expected that the temperature oscillatory behavior can be observed above 100 K.[25]

The hydrodynamic response was numerically predicted in gas fluids for a small Knudsen number using the traditional Navier−Stokes equation. Analogous to a rarefied gas[26] and a viscous electron flow,[27] phonon hydrodynamic transport can be captured in solids based on non-Fourier heat transport models such as the Maxwell−Cattaneo−Vernotte (MCV) equation,[28,29] dual-phase-lag (DPL),[30−32] and the Guyer−Krumhansl equation (GKE).[26,33] In graphitic materials, the non-Fourier feature provides a detailed theoretical description of second sound propagation and phonon hydrodynamic transport. However, the analytical solutions of phonon BTE are crucial for the investigation of the heat transport regime in the mesoscopic scale. Non-Fourier phonon transport models cannot capture the nonequilibrium effect in a confined space. On the other hand, the boundary temperature jump (BTJ) condition is still applicable to probe gas and phonon flow in the slip regime.[34−37] BTJ offers an accurate way to take into account nonequilibrium effects due to phonon boundary confinements.[34] Accordingly, the combination between non-Fourier heat-transfer models and BTJ condition allows a new insight into the identification of hydrodynamic heat transport on the further side of Fourier's law.

This work aims to highlight the physical picture of hydrodynamic heat transport and the method to classify different thermal transport regimes. In principle, the ballistic transport was directly observed in heat pulse propagation at low temperatures. To avoid the ballistic transport, we focus on high temperatures, which provides a promising potential for thermal design and phonon manipulation in 2D materials. To establish a consistent theoretical prediction with an experimental setup, we consider the BTJ condition at the top boundary (hot spot), and an adiabatic boundary with diffuse scattering is applied for the lateral surfaces, while a constant temperature is imposed to the bottom boundary (cold source).

The paper is organized as follow as: the non-Fourier features for ultrafast thermal transport including the DPL and MCV models are introduced in Section 2. The boundary condition of the temperature jump is derived in Section 3. In Section 4, the proposed scheme is validated for transient phonon transport. In addition, we demonstrate that the present non-Fourier model is able to describe the hydrodynamic heat transport. Section 4 is devoted for concluding remarks. Finically, the present scheme based on the finite element method (FEM) with ab initio coefficients is provided in Section 5.

## 2. ULTRAFAST NON-FOURIER HEAT TRANSPORT

The DPL model was treated for the investigation of heat transfer in semiconductors,[38] layered correlated materials,[39] and laser heating in biological tissues (e.g., bio-heat transfer).[40] The DPL model characterizes the thermal lagging response in ultrafast heat transport by introducing two-phase lags $\tau_T$ and $\tau_q$ which are the phase lag of the temperature and the phase lag of the heat flux, respectively, and $Z = \frac{\tau_T}{\tau_q}$ represents the phase lag ratios.[31,41]

The starting point, to describe the lagging thermal response in low-dimensional systems, is the following expression given by Tzou[30,31]

$$q(r, t + \tau_q) = -\kappa \nabla T(r, t + \tau_T) \tag{1}$$

where $q = q(r,t)$ is the heat flux, $t$ is the time scale, $\kappa$ is the bulk thermal conductivity, and $T = T(r,t)$ is the temperature field. Here, the DPL model predicts a non-Fourier effect including two-time lags to access the ultrafast carrier dynamics. For short relaxation times $\tau_q$ and $\tau_t$ (ultrafast time scale), the derivation of eq 1 leads to

$$q(r, t) + \tau_q \frac{\partial q(r, t)}{\partial t} = -\kappa \nabla T(r, t) - \kappa \tau_T \frac{\partial}{\partial t} \nabla T(r, t) \tag{2}$$

The differential equation of the temperature evolution can be obtained by coupling eq 2 with the conservation of energy

$$C \frac{\partial T(r, t)}{\partial t} + \nabla \cdot q(r, t) = 0 \tag{3}$$

where $C$ is the volumetric heat capacity. The ultrafast non-Fourier thermal transport along the $x$- and $y$-directions can be written as

$$\tau_q \frac{\partial^2 T}{\partial t^2} + \frac{\partial T}{\partial t} = \frac{\kappa}{C}(\nabla^2 T) + \tau_T \frac{\kappa}{C} \frac{\partial}{\partial t}(\nabla^2 T) \tag{4}$$

The DPL model provides a crucial correction in the thermal response by adding two-phase lags in Fourier's law. From a point of view of carrier dynamics, the DPL introduces the causality relation between the gradient of temperature and heat flux. The causal behavior is achieved by both the temperature gradient as the cause of heat flux ($\tau_q > \tau_T$) and the heat flux as the cause of the temperature gradient ($\tau_q < \tau_T$). Therefore, the DPL model treats the heat propagation at the nanoscale regime by describing the lagging behavior and nonlocal effects.[30] In terms of phonon scattering mechanisms, $\tau_q$ and $\tau_T$ have the same physical picture of resistive ($R$) phonon scattering time $\tau_R$ and normal ($N$) phonon scattering time $\tau_N$, respectively. For the mesoscopic approach of non-Fourier heat transport, DPL provides a unified mathematical description analogous to the Guyer−Krumhansl


https://doi.org/10.1021/acsomega.3c02558
ACS Omega 2023, 8, 23964−23974

equation with regard to the theory of phonon gas.[31] For $Z = 0$, the DPL model reduces exactly to the single-phase lag (SPL) known as the MCV equation.[42,43] The heat flux distribution into the MCV equation for 2D transient heat transport is derived from eq 2 as

$$q + \tau_R \frac{\partial q}{\partial t} = -\kappa \nabla T \tag{5}$$

Equation 5 is adapted to investigate the ultrafast non-Fourier heat transport in extremely low nanosystems. In the diffusive limit, where *R*-scattering events are fully dominated, both eqs 2 and 5 recover Fourier's law. From a mathematical point of view, the MCV equation predicts an ideal hydrodynamic regime manifested by the dominance of *N* scattering events (i.e., $\tau_T = 0$). Through a similar derivation of eq 2, the differential equation of the temperature can be written as

$$\tau_R \frac{\partial^2 T}{\partial t^2} + \frac{\partial T}{\partial t} = \frac{\kappa}{C}(\nabla^2 T) \tag{6}$$

The MCV heat equation type represents an enhanced formalism of Fourier's law, including nonequilibrium effects associated with the theoretical detection of second sound. Experimentally, the observation of the second sound occurs when momentum−conservation phonon *N* scattering dominates, leading to the hydrodynamic regime. From a theoretical point of view, the hydrodynamic heat transport takes place when phonon−phonon *N*-scattering events are stronger than the boundary scattering and weaker than the *R*-scattering events. The inverse of the pulse duration (external pulse input), $\tau_{theo}^{-1}$, should be smaller than the *N*-scattering rate but greater than the *R*-scattering rate. The required condition for second sound propagation can be simplified as

$$\tau_N^{-1} > \tau_{theo}^{-1} > \tau_R^{-1} \tag{7}$$

Generally, the temperature oscillation behavior reflects the wave-like motion where the heat pulse is transmitted by *N*-scattering. The velocity of second sound, $v_{ss}$, can be estimated as[31,43,44]

$$v_{ss} = \sqrt{\frac{\alpha}{\tau_R}} \tag{8}$$

where $\alpha$ represents the thermal diffusivity ratio of thermal conductivity to heat capacity (see Supporting Information S1). In principle, to observe a drifting second sound, the material will exhibit a ballistic (or quasiballistic) to hydrodynamic crossover. The hydrodynamic regime is significantly dependent on the contribution of the diffuse boundary scattering combined with the *N*-scattering events. Therefore, one would need an accurate boundary condition to distinguish the hydrodynamic regime from the other transport regimes.

## 3. BOUNDARY TREATMENT

Non-Fourier effects included in hyperbolic type correspond to the wave-like flow of the phonon Boltzmann solution. To clearly observe three different transport regimes, an accurate boundary condition should be attributed to the heat pulse propagation. The crossover of quasi-ballistic to hydrodynamic is usually determined based on the spatial Knudsen number, $Kn_R = \frac{\Lambda}{L_h}$, where $\Lambda$ is the average mean free path (MFP) and $L_h$ is the characteristic length.[13] Typically, the hydrodynamic heat transport is observed when the spatial Knudsen number is less than 0.3.[34] The analytical solutions of phonon BTE (e.g., DPL and MCV) are not sufficient to capture the crossover phenomena. It still requires a suitable slip boundary condition for the description of the transient heat pulse. Strong nonequilibrium effects that are seriously influenced by phonon boundary scattering still needed a further understanding to realize a clear interpretation of ultrafast heat response. Particularly, the BTJ condition is useful for a transitional regime with respect to Knudsen's theory.[34−37] BTJ can be derived from steady-state phonon BTE (see Supporting Information S2).

$$T - T_h = -\frac{2}{3} C \Lambda \left.\frac{\partial T}{\partial y}\right|_{Y=0} \tag{9}$$

where $T_h$ is the hot spot temperature defined as $T_h = T_0 + \Delta T$, where $T_0$ is the initial temperature and $\Delta T$ is the imposed temperature difference. Here, *C* is a dimensionless coefficient defined in terms of Ziman specularity *p*[44]

$$C = \frac{1 + p}{1 - p} \tag{10}$$

Equation 9 represents a nonequilibrium slip boundary condition applied at the top wall as shown in Figure 1. Near

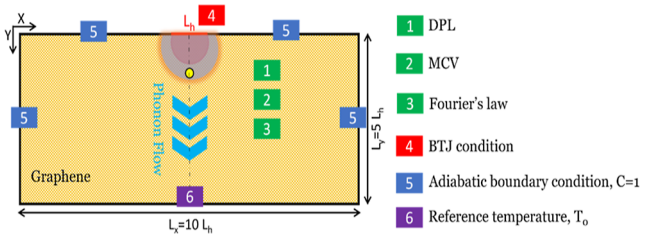


**Figure 1.** Schematic of phonon transport and boundary conditions used for the ab initio FEM simulations. The yellow circle denotes the detector located along the *Y*-direction.

the boundary, strong nonequilibrium thermodynamic effects lead to temperature jumps due to the random walk behavior of phonon interactions. At the early transition regime, nonlocal terms of temperature gradient impose additional difficulty in capturing ultrafast heat transport at a Knudsen number about 1. In this way, the BTJ condition describes well the crossover regime of heat transport from diffusive (Fourier's solution) to nonequilibrium (nondiffusive) phenomena occurring at the early heating stage. Furthermore, BTJ includes both temporal and spatial information providing crucial correction of the constitutive non-Fourier heat models derived based on mesoscopic equations. Therefore, the coupling of both non-Fourier equations and BTJ condition will be able to investigate the thermal response in low-dimensional systems and ultrafast time scales. In this work, the bottom wall is maintained at $T_0$, and an adiabatic boundary condition with fully diffuse boundary scattering, $C = 1$, is considered for the lateral surface. As mentioned in the literature,[11,16] the adiabatic boundary condition seems to be significant for the observation of second sound propagation with respect to the heat pulse experiment. At the initial moment $t_0$, the temperature is $T_0$ in the whole domain. At a certain time, $t + \Delta t$, the temperature at the top boundary is suddenly increased to $T_h$. In this work, the dimension of the simulated graphene sample is 10 $\mu$m × 5 $\mu$m, and $L_h$ is the nanoscale hot spot. The heating problem describes a transient heat pulse propagation from hot spot temperature using a


https://doi.org/10.1021/acsomega.3c02558
ACS Omega 2023, 8, 23964−23974

coupled ab initio FEM scheme. The thermal properties of graphene are involved in the literature with respect to ab initio BTE calculations (Table 1).[15,41]

**Table 1. Ab Initio Phonon Properties of Graphene[15,41]**

| thermal parameters | $T$ = 80 K | $T$ = 100 K | $T$ = 300 K |
|---|---|---|---|
| $\kappa$ (W m$^{-1}$K$^{-1}$) | 4.3 × 10$^3$ | 5 × 10$^3$ | 3.8 × 10$^3$ |
| $C$ (J m$^{-3}$k$^{-1}$) | 2.3 × 10$^5$ | 3.3 × 10$^5$ | 1.6 × 10$^6$ |
| $\tau_q$ (ps) | 1800 | 300 | 2.43 |
| $\tau_T$ (ps) | 3 | 2.5 | 0.89 |
| $Z$ | 0.0016 | 0.083 | 0.36 |

The present macroscopic model is a solution to BTE with phonon properties based on microscopic methods. The aim of this work is (1) to testify the numerical accuracy of non-Fourier features, (2) to understand the propagation of the heat wave, and (3) to distinguish the hydrodynamic transport regime and estimate the second sound velocity. In this context, this present ab initio FEM framework is the unique existing scheme to calculate the second sound velocity using non-Fourier formalism based on the finite element method. This work contributes to an efficient methodology for deeper understanding of size effect hydrodynamic heat transport in graphene.

## 4. RESULTS AND DISCUSSION

**4.1. Transient Heat Transport: Methodology Validation.** The investigation of transient nanoscale heat transport by directly solving the phonon BTE with full scattering terms is computationally expensive. As is already known, the traditional numerical methods fail to describe the spatial−temporal evolution when the MPF is very small compared to the system characteristic time and length. The discrete unified gas kinetic scheme (DUGKS), a finite volume method, was recently developed to solve the phonon BTE for multiscale heat transport with different boundary conditions.[12,45,46] Several numerical results have demonstrated that DUGKS has an advantage of modeling non-Fourier thermal transport with respect to phonon BTE. In a previous work, DUGKS provides an efficient and stable scheme for solving the phonon BTE under Callaway's model.[12] Inspired by recent works, we have developed a novel ab initio FEM scheme which is able to handle phonon transport problems with low computational cost. To validate the present methodology, DPL, MCV, and Fourier's law are compared with DUGKS for 1D transient thermal transport in graphene with the length $L$ (corresponding to $L_h$). Initially ($t$ = 0), the temperature of the sample is kept fixed at $T_L$ = 299.5 K, and suddenly, the temperature increases at the left boundary $T_H$ = 300.5 K. The ab initio data for $T$ = 300 K are shown in Table1. In this section, we attempt to testify the performance of the ab initio FEM scheme. The DPL model reproduces the DUGKS profile as shown in Figure 2a. The dual-phase lag model includes two phase lags introducing a causality relation between the onset of heat flux and the temperature gradient. The most prominent aspect of the DPL model is the prediction of lagging behavior and nonlocalities. However, MCV fails to reproduce DUGKS because MCV includes only one phase lag of the heat flux without considering the phase lag of the temperature gradient. Therefore, MCV overestimates the propagation of heat. This overestimation of the MCV profile has also been observed in heat transport modeling, where the Knudsen number is high. Although MCV provides an enhancement over Fourier's law, the present DPL model is more accurate with respect to DUGKS.

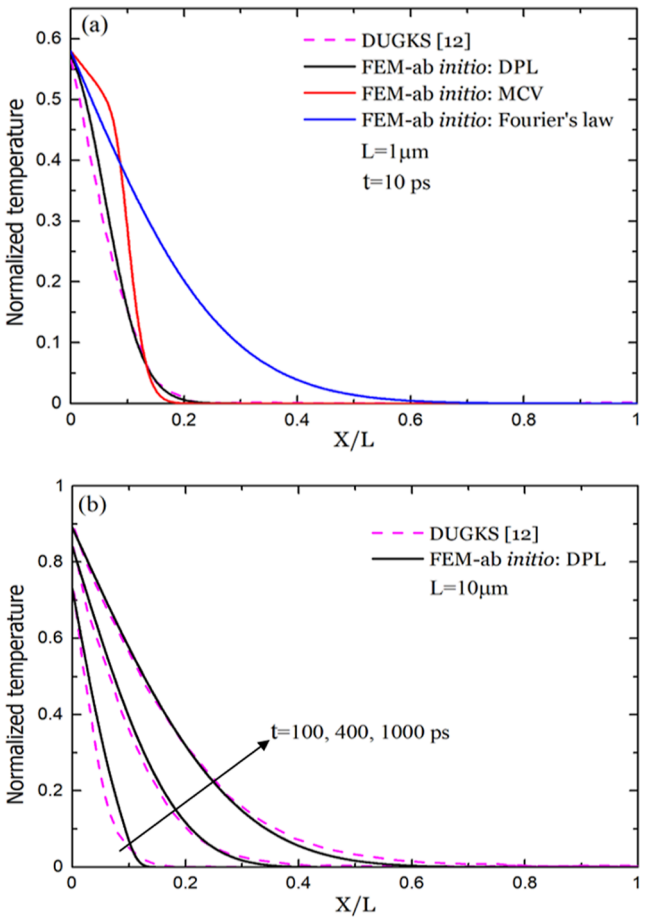


**Figure 2.** Distribution of dimensionless temperature in graphene. (a) $L$ = 1 $\mu$m and (b) $L$ = 10 $\mu$m.

Fourier's law is not able to describe the thermal transport at an ultrafast time scale of 10 ps. Figure 2b shows the temperature distributions in graphene with length $L$ = 10 $\mu$m at different time scales ($t$ = 100, 400, and 1000 ps). DPL predicts the spatial−temporal evolution of temperature similarly as obtained by DUGKS. The present DPL gives a global agreement with DUGKS, especially at $t$ = 100 and 400 ps. The FEM ab initio scheme for DPL is a computationally low-cost framework, which ensures a good accuracy based on dense mesh resolution.

**4.2. Hydrodynamic Heat Transport.** *4.2.1. Breakdown of Fourier's Law.* The hydrodynamic transport originates from its analogy with the viscous effect in a rarefied gas flow. The phonon hydrodynamic phenomena refer to heat propagation in characteristic length, $L_h$, experiencing a minimum with respect to MFP, which is called the phonon Knudsen minimum.[23,47] The Knudsen minimum was confirmed experimentally by Knudsen and then studied numerically by solving the fluid BTE.[48] In a recent literature study, theoretical calculation demonstrates that hydrodynamic transport occurs when 0.1 ≤ $Kn$ ≤ 10 for germanium telluride (GeTe).[49] In addition, the hydrodynamic regime is also observed in bismuth at $T$ = 3.5 K for Knudsen number about 0.58. Therefore, the Knudsen number is a critical macroscopic quantity for capturing the transition between hydrodynamic and diffusive regimes.

In this section, we carry out 2D transient heat transport in graphene using a non-Fourier response for the evidence of hydrodynamic regime. We highlight the transition between hydrodynamic and diffusive regimes by considering the effect of


https://doi.org/10.1021/acsomega.3c02558
ACS Omega 2023, 8, 23964−23974

macroscopic quantities such as second sound velocity and the spatial Knudsen number. Essentially, we address the thermal wave behavior at 80 K through a hydrodynamic−diffusive crossover. The present scheme guarantees a low computational cost of non-Fourier heat modeling at the mesoscopic level. In this work, the dimensionless temperature is calculated using $T^* = \frac{(T_{max} - T_0)}{\Delta T}$ obtained by solving DPL, MCV, and Fourier's law, where $T_{max}$ is the maximum value in the temperature distribution.

Figure 3 shows the temperature evolution along the $Y$-axis at $t$ = 1 ns for different Knudsen numbers. DPL predicts the

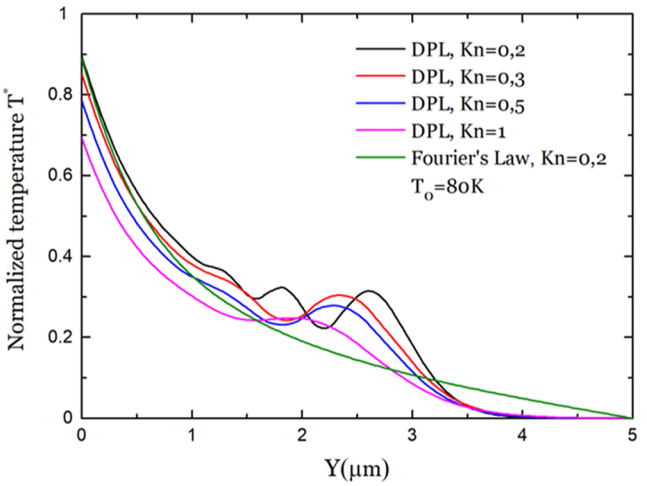


**Figure 3.** Distribution of dimensionless temperature along the $Y$-direction at $T_0$ = 80 K for different Knudsen numbers at $t$ = 1 ns.

hydrodynamic regime in graphene by providing a theoretical description of thermal wave-like flow beyond Fourier's law. The phonon hydrodynamic transport is significantly dominated at a spatial $Kn$ smaller than 0.3, which is confirmed in the literature.[34] At $T_0$ = 80 K, the temperature oscillations are notably observed when the Knudsen number is around 0.2. The classical Fourier's law is not suitable to probe nondiffusive heat transport. Using Fourier's law, the heat pulse cannot propagate as a damped wave, denoting a diffusive regime where $R$-scattering dominates and destroys the momentum. Non-Fourier schemes are therefore essential for ultrafast heat transport in 2D materials. In the hydrodynamic regime, the heat pulse propagates as a wave-like behavior transmitted by $N$-scattering, similar to the viscous term in Navier−Stokes's equation. In general, the oscillating response indicates that a wave-like motion occurs in the quasiballistic heat pulse or the hydrodynamic regime. It is clearly observed in Figure 4 that both DPL and MCV describe a temperature oscillation response that would match to a certain propagation velocity. The heat velocity propagation, $v = \frac{y}{\Delta t}$, serves an essential way to distinguish different transport regimes. Here, the transient thermal decay is controlled by a detector along the $y$-direction. By using eq 8, ab initio calculations estimate that the second sound velocity is 3222 m/s at $T_0$ = 80 K. For $Y$ = 1 $\mu$m and according to the DPL prediction, the first three peaks indicated by their arrival times $t_1$ = 0.44 ns, $t_2$ = 0.63 ns, and $t_3$ = 0.83 ns, give $v_1$ = 5263 and $v_2$ = 5000 m/s. The input heat pulse (corresponds to $t_1$) starts to divide into three peaks, corresponding to quasiballistic and second sound pulses. The four-temperature peak arrives at $t_4$ = 1.12 ns corresponding to

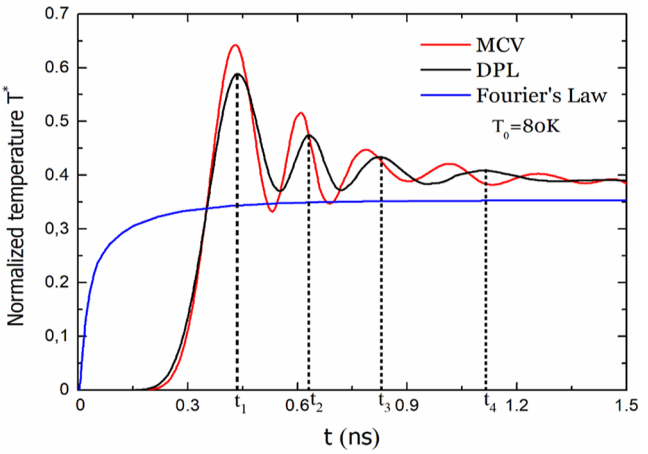


**Figure 4.** Distribution of dimensionless temperature in graphene at $T_0$ = 80 K using DPL, MCV, and Fourier's law for $Kn$ = 0.2 at $t$ = 1.5 ns around the position ($X$ = 5 $\mu$m and $Y$ = 1 $\mu$m).

the propagation speed $v_3 = \frac{Y}{t_4 - t_3}$ = 3448 m/s, which is close to $v_{ss}$ estimated by ab initio calculations. Consequently, the second and third peaks are quasiballistic pulse; however, the fourth temperature peak corresponds to the second sound pulse. For MCV, the five temperature peaks are denoted by their arrival times, $t_1$ = 0.43 ns, $t_2$ = 0.6 ns, $t_3$ = 0.78, $t_4$ = 1 ns, and $t_5$ = 1.26 ns, corresponding to propagation speeds $v_1$ = 5882 m/s, $v_2$ = 5555 m/s, $v_3$ = 4545 m/s, and $v_4$ = 3846 m/s. For comparison, DPL is computationally more accurate than MCV with respect to ab initio estimations because DPL includes dual relaxation times that describe the phonon−phonon scattering events. MCV overestimates the temperature oscillation due to the negligible contribution of $\tau_T$, which is not correct according to the ab initio data (i.e., $\tau_T \neq 0$). The solution of Fourier's law cannot predict the wave-like flow and describes only a diffusive regime where the heat pulse cannot propagate. Therefore, three different regimes are distinguished based on velocity propagation. In the quasiballistic regime, the heat pulse propagates faster than the second sound velocity. Then, the hydrodynamic regime takes place in the sample with propagation speed close to $v_{ss}$. In the diffusive regime, the heat pulse is significantly damped by $R$-scattering and cannot propagate as an oscillating wave, which can also be seen in Figure 5. In this work, we have further

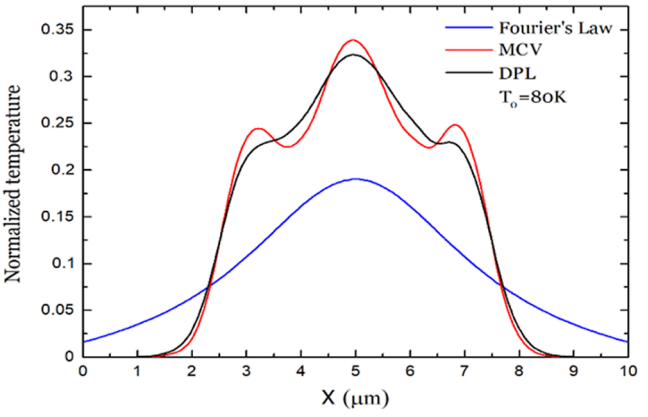


**Figure 5.** Nondimensional temperature along the $X$-direction in graphene at $T_0$ = 80 K using DPL, MCV, and Fourier's law for $Kn$ = 0.2 and $Y$ = 1 $\mu$m at $t$ = 1 ns.



https://doi.org/10.1021/acsomega.3c02558
ACS Omega 2023, 8, 23964−23974

mapped the transient heat propagation by measuring the temperature contours within the computational domain. Here, the ab initio FEM solver is used to plot the surface temperature through solving the DPL and Fourier's law. Figure 6a shows the

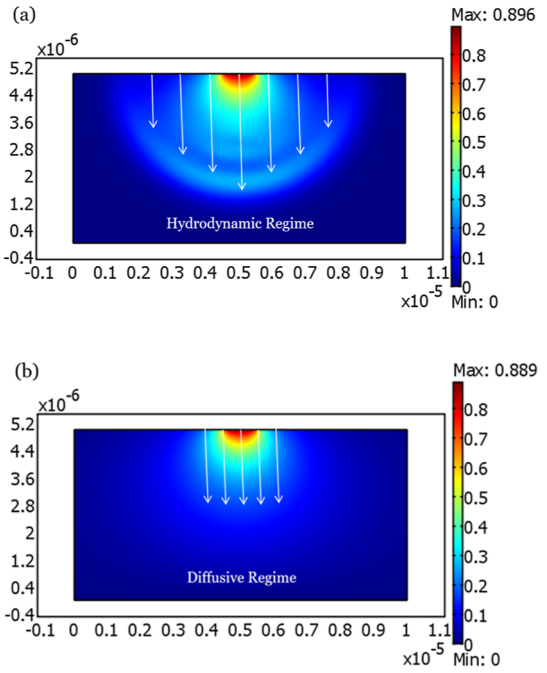


**Figure 6.** Surface temperature detection in graphene around $T_0 = 80$ K at $t = 1.2$ ns. (a) DPL model and (b) Fourier's law. Fourier's solution describes a uniform temperature decay denoting the diffusive-like regime.

temperature map evolution using the DPL model at $t = 1.2$ ns. The hydrodynamic regime is distinctly different from the usual diffusive transport probed by Fourier's law. Fundamentally, the breakdown of the classical heat equation can be explained by the fact that Fourier's law cannot predict a nonequilibrium thermodynamic effect in low-dimensional systems. In the hydrodynamic regime, phonons display a nonuniform temperature profile, and the heat is transported without important damping. In diffusive transport, the heat is mainly influenced by intrinsic resistive scattering (Umklapp scattering), leading to the uniform shape as can be seen in Figure 6b. The transient heat propagation from the hot spot is completely different with respect to Fourier's and non-Fourier regime. The thermal mapping technique shows a hydrodynamic transport like fluid flow. At the very early stage, the heat propagation is an ultrafast heat transport (ballistic or quasiballistic) influenced by *N*-scattering events. Thereafter, phonon exhibits nonballistic transport (hydrodynamic or diffusive), which mainly depends on the scattering rates. For the DPL model, to guarantee a hydrodynamic transport, the phase lag ratios "*Z*" should be small enough. The term "*Z*", included in DPL, aims to control the damping featured in transient heat propagation. The coupled ab initio FEM scheme successfully captures the hydrodynamic regime based on non-Fourier heat transport.

*4.2.2. Size Effects on Hydrodynamic Heat Transport.* Recent experimental and theoretical studies have focused on the emergence of the hydrodynamic transport.[50−52] To further clarify the oscillating behavior, we study 2D heat transport along the *x*-direction for different positions along the *y*-direction. The spatial Knudsen number is fixed at 0.2 to guarantee an observation of hydrodynamic-to-diffusive crossover. Figure 7 shows the comparison of the thermal decay curves predicted by

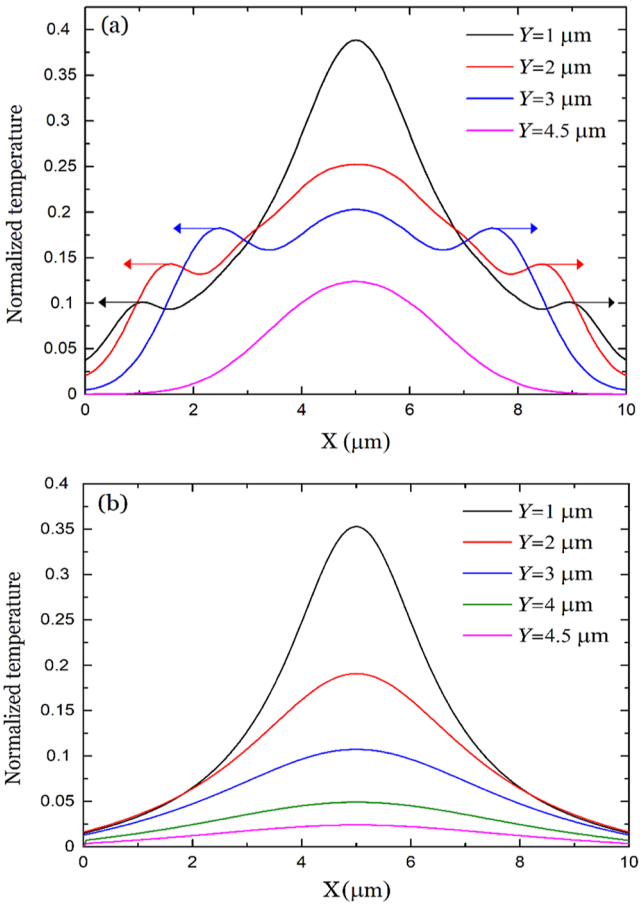


**Figure 7.** Nondimensional temperature along the *X*-direction at $T_0 = 80$ K for $Kn = 0.2$ around different *Y*-positions at $t = 1.5$ ns. (a) DPL model and (b) Fourier's law. The arrows indicate the direction of thermal wave response.

DPL and Fourier's law at $T_0 = 80$ K for the arrival time $t = 1.5$ ns. Figure 7a illustrates the temperature profiles by using the DPL model for different sizes around $T_0 = 80$ K. Notably, the thermal wave-like response occurs for $Y = 1$, 2, and 3 $\mu$m with different amplitudes. The temperature decay is no longer exponential and displays an oscillating response, which denotes a nondiffusive regime. For $Y = 4.5$ $\mu$m, the wave-like behavior disappears, indicating that the transport regime shifts to diffusive. Fourier's law fails completely in describing any oscillating behavior in the computational domain. As expected, Fourier's solution describes a diffusive regime where the heat pulse is kept fixed at the center of the sample as shown in Figure 7b. Phonon hydrodynamic transport is a collective behavior with the same drift velocity along a finite size. In the actual hydrodynamic heat flow, *N*-scattering gives a strong viscous damping and an oscillating motion of the temperature destitution. Here, we consider a transient heat transport where the size effect comes from the top boundary by changing the characteristic length $L_h$ along the *y*-direction. A uniform spatial mesh is used, and an extremely fine mesh is also considered for the top boundary (see Supporting Information S3). In order to be closer to the real situation of heat dissipation from the hot spot, the computational domain is given by finite width and more realistic boundary conditions. Equation 9 denotes that the cross-plane


https://doi.org/10.1021/acsomega.3c02558
ACS Omega 2023, 8, 23964−23974

temperature jumps close to the heat source. Due to the strong nonlocal effects near the hot spot temperature (localized heat source), a significant mismatch occurs between the isotropic Bose−Einstein distribution and the displaced phonon distribution. Therefore, the BTJ condition is mandatory, for instance, in predicting the nonlinearity of temperature close to the heat source. Similar to Navier−Stokes hydrodynamic equation, the DPL model describes the phonon viscous flow via the nonlocal term of the heat flux (the right side of eq 4). Figure 8 plots the temperature distribution using the DPL model at $t$ = 1 ns for different $L_h$. With increasing heat source size, the hydrodynamic phonon transport becomes clear. As shown in Figure 8a, the temperature becomes nonuniform and shows an oscillating response. For $L_h$ = 1000, 1500, and 2000 nm, the temperature oscillating response becomes significantly nonexponential, indicating the emergence of hydrodynamic heat flow as shown in Figure 8b−d. When the heat source size is small enough, the heat transport is quasiballistic because phonons do not exhibit a sufficiently normal scattering as shown in Figure 8e (see Supporting Information S3 for further discussion of this point).

**4.3. Driftless Second Sound.** Several experimental and theoretical investigation have classified another type of second sound, named "driftless second sound".[53−56] The driftless second sound is not a hydrodynamic transport. More recently, the driftless second sound requires a high-frequency excitation.[56] However, drifting second sound (hydrodynamic transport) requires sufficient momentum conservation. Here, we focus on the detection of driftless second sound detection at $T_0$ = 100 K. Figure 9 illustrates the effect of the Knudsen number in cross-plane heat transport at $T_0$ = 100 K during time and size scaling. The thermal wave response is clearly detected around the positions $Y$ = 0.7, $Y$ = 1, and $Y$ = 1.5 $\mu$m when $Kn$ = 0.1. For $Y$ = 0.5 $\mu$m, we observe an overshooting temperature behavior due to boundary scattering, indicating that the dominant transport is quasiballistic as shown in Figure 9a. The thermal wave can also occur in the quasiballistic regime but with a small drift velocity. As the size increases ($Y$ = 0.7 $\mu$m), phonons experience gradually less boundary scattering, leading to a significant temperature oscillation, which indicates that the transport regime is switched from quasiballistic to second sound. At $T_0$ = 100 K, ab initio data estimates a second sound velocity of around 7106 m/s. For the DPL model, the second, third, and fourth temperature peaks arrive at $t_2$ = 0.25 ns, $t_3$ = 0.32 ns, and $t_4$ = 0.42 ns, respectively, corresponding to propagation velocity $v_1 = \frac{0.7\ \mu m}{0.07\ ns}$ = 10,000 m/s and $v_2 = \frac{0.7\ \mu m}{0.1\ ns}$ = 7000 m/s. Therefore, the first two peak temperatures are quasiballistic heat pulses; however, the fourth temperature peak is essentially the second sound pulse. For $Y$ = 0.7 $\mu$m, three different regimes are clearly distinguished: (1) quasiballistic regime, (2) driftless second sound ($t = t_4$), and (3) diffusive regime ($t > t_4$). The second sound disappears progressively with increasing size, and only quasiballistic−diffusive crossover is detected. For $Y$ = 1 and 1.5 $\mu$m, the calculated propagation velocities are 12.500 and 13.636 m/s, respectively. This is because $R$-scattering dominates with increasing sample size and progressively destroys the momentum conservation. For $Y$ = 2 $\mu$m, the wave oscillating response is much weaker compared with $Y$ = 1.5 $\mu$m, which indicates that the transport regime is shifting to diffusive rather than quasiballistic. Table 2 summarizes the drifting and driftless second sound in graphene at $T_0$ = 80 and 100 K. From Figures 4 and 9a, it is remarkably seen that both the drifting and driftless second sound strongly depend on the sample size and phonon

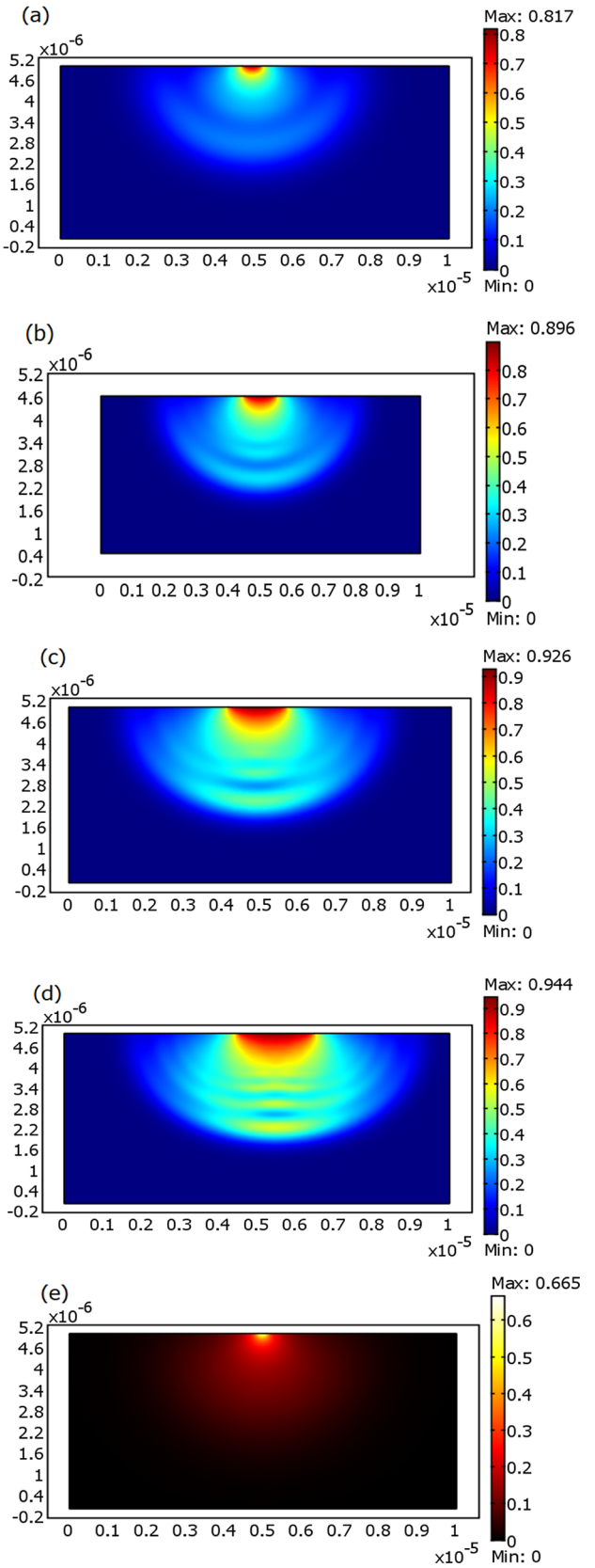


**Figure 8.** Surface temperature detection in graphene at $T_0$ = 80 K at $t$ = 1 ns for different $L_h$. (a) 500, (b) 1000, (c) 1500, (d) 2000, and (e) 200 nm.

scattering mechanisms. At $T_0$ = 80 K, the hydrodynamic regime (drifting second sound) is detected for $Y$ = 1 $\mu$m; however, the



https://doi.org/10.1021/acsomega.3c02558
ACS Omega 2023, 8, 23964−23974

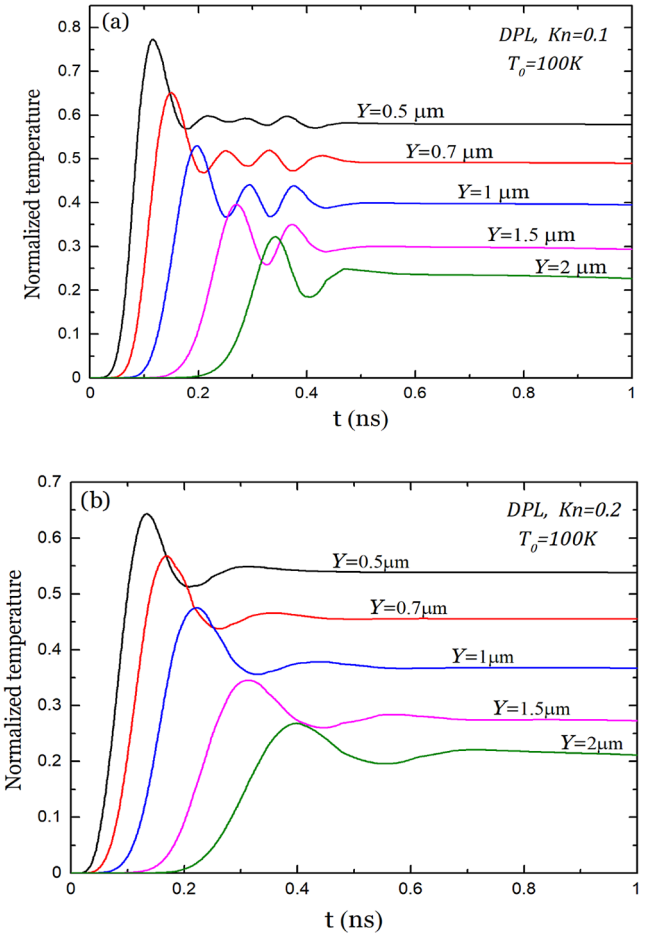


**Figure 9.** Transient thermal transport in graphene at $T_0$ = 100 K using the DPL model. Dimensionless temperature with different *Y*-positions: (a) *Kn* = 0.1 and (b) *Kn* = 0.2.

**Table 2. Drifting and Driftless Second Sound for Graphene**

| velocity (m/s) | drifting | driftless |
|---|---|---|
| second sound at $T_0$ = 80 K | 2165 (55), 2841 (14), 3448 (DPL) | 5851 (55), 5000 (DPL) |
| second sound at $T_0$ = 100 K | 2360 (55) | 6214 (55), 7106 (DPL) |

driftless second sound occurs when the size is about 0.7 $\mu$m at $T_0$ = 100 K. When the temperature increases, the *N*-scattering rate also increases, providing longer phonon trajectories due to random walk transport. Figure 9b shows the spatial and temporal evolution of the temperature in graphene at $T_0$ = 100 K for *Kn* = 0.2. It is clear that the temperature oscillations are relatively weaker along the sample. The quasiballistic-to-driftless second sound crossover starts disappearing with increasing *Kn*. The transition between quasiballistic and driftless second sound can arise if the spatial Knudsen number is smaller than 0.3. This can be explained by the boundary scattering effect on the heat propagation pulse. As *Kn* increases, the lateral boundary scattering (extrinsic resistive scattering) leads to momentum loss, and therefore, the transport regime shifts from quasiballistic to diffusive regime without second sound transition. With increasing *Kn*, the temperature profiles of quasiballistic pulses do not differ very much, although their amplitudes reduce. Figure 10 shows the normalized temperature change with respect to time, d$T$/d$t$, at $T_0$ = 80 K and $T_0$ = 100 K. At $T_0$ = 80 K, there is

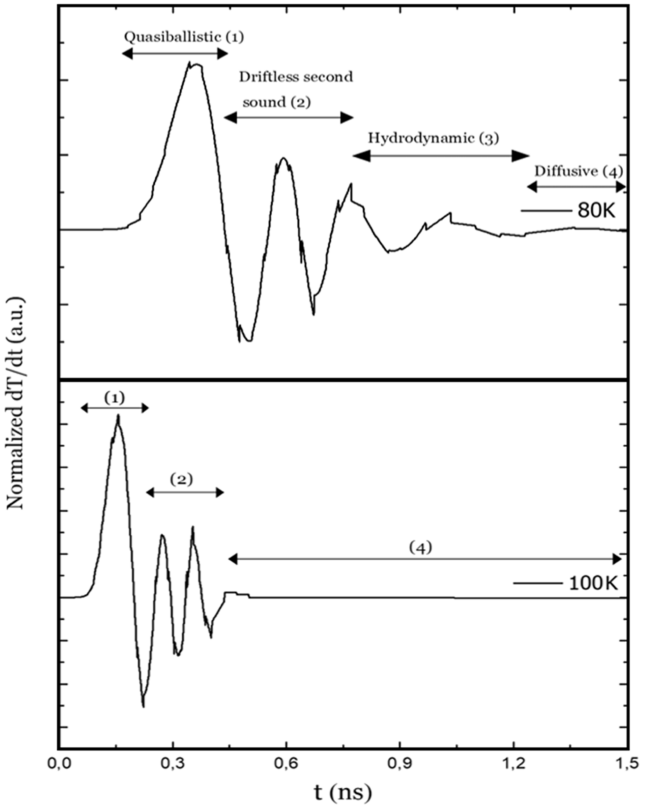


**Figure 10.** Normalized d$T$/d$t$ profiles using DPL for $Y$ = 1 $\mu$m at $T_0$ = 80 and 100 K.

clear evidence of hydrodynamic heat transport indicated by the transient cooling feature. The negative temperature peaks are induced by many *N*-scattering events analogous to pressure pulse in a gas flow. In practical situations, the cooling process cannot occur in both ballistic and diffusive regimes.[16] Quite surprisingly, the negative temperature signal appears at $T_0$ = 100 K for $Y$ = 1 $\mu$m, indicating the existence of a heat wave phenomenon. Therefore, the second sound phenomena can also be observed in ultrafast heat transport (i.e., high-frequency or driftless second sound). The velocity of drifting and driftless second sound differs from each other, and the driftless second sound is expected to propagate faster than the drifting second sound. In this case, the driftless second sound is a transition between quasiballistic and diffusive regimes where the dominance of *N*-scattering is not an essential condition. In other words, the driftless second sound is a crossover regime which requires a higher thermal excitation. Unexpectedly, the thermal fluctuation designated by negative change of temperature field confirms the occurrence of wave-like behavior without the dominance of *N*-scattering events. The negative temperature is observed for $Y$ = 0.7 $\mu$m and even for $Y$ = 1.5 $\mu$m as can be seen in Figure 11. The negative peaks become clear for the size of 0.7 $\mu$m because the thermal wave-like transport dominates owing to drifting second sound propagation. The drifting second sound may happen only in the hydrodynamic regime when the dominance of *N*-scattering is mandatory, while driftless second sound allows a direct manifestation of heat waves through its oscillating behavior. The d$T$/d$t$ peaks prove that the thermal transport regime changes from quasiballistic to driftless second sound (crossover regime) for $Y$ = 0.7 $\mu$m; however, the quasiballistic transport weakens for $Y$ = 1.5 $\mu$m. In this case, the cooling behavior can be achieved by both drifting


https://doi.org/10.1021/acsomega.3c02558
ACS Omega 2023, 8, 23964−23974

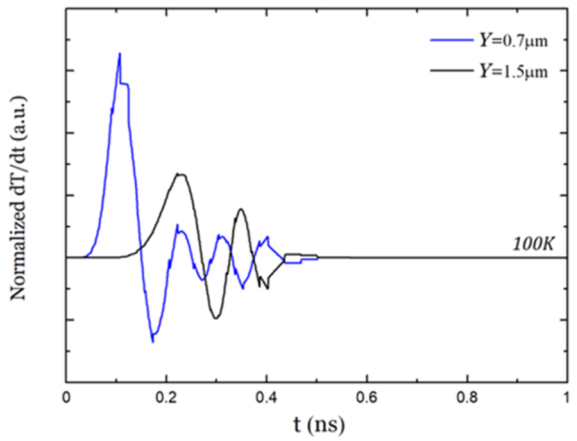


**Figure 11.** Normalized d$T$/d$t$ profiles measured based on DPL at $T_0$ = 100 K around different $Y$-positions.

and driftless second sound. In other words, driftless second sound does not lie in the hydrodynamic window but contributes more to heat wave-like propagation within the graphene sample. The driftless second sound seems to make sense at higher temperatures with larger system size, which is very promising for thermal management applications and cooling of electronics devices.

## 5. CONCLUSIONS

In summary, we investigated the hydrodynamic heat transport in graphene at $T$ = 80 and 100 K using non-Fourier behavior. The 2D heat transport was carried out based on the ab initio FEM frameworks by solving the hyperbolic wave equation with respect to phase lag theory. The wave-like heat transport can appear due to (1) drifting second sound where normal scattering events dominate (hydrodynamic regime) and (2) driftless second sound, which do not recommend the dominance of $N$-scattering. The drifting second sound is manifested by the ballistic (or quasiballistic) to hydrodynamic transition that depends on the Knudsen number. Indeed, to observe a drifting second sound, the spatial Knudsen number should be less than 0.3 (Knudsen minimum). However, a driftless second sound can occur without $N$-scattering damping, which opens up a new picture of heat wave propagation at highest temperatures and interesting opportunities to manipulate heat in next-generation nanoelectronic devices. From a theoretical point of view, to clearly identify the wave-like heat transport, the d$T$/d$t$ profile should indicate a negative peak, denoting the cooling feature. In future work, we will focus on hydrodynamic transport in other materials for a deeper understanding of wave-like heat flow at highest temperature, which is an emerging topic in the physics behind the breakdown of Fourier's law.

## 6. METHOD: FEM AB INITIO SOLVER

The 2D heat transport is carried out using the finite element method by solving DPL, MCV, and Fourier's law. For the FEM ab initio scheme, all the thermal parameters included in HHEs are ab initio coefficients.

The finite element method aims to couple the non-Fourier heat models with the slip boundary conditions based on ab initio inputs. During the simulations, a dense mesh is considered in the whole domain, and an extremely finer spatial mesh is applied at the top boundary. The transient heat transport was computed with 911 triangular meshes and a time step of 1 ps. In consequence, the present scheme describes the temporal and spatial thermal transport within the 2D geometry. We have demonstrated that the thermal wave-like transport can be computationally observed using non-Fourier heat transfer models as illustrated in Figure 12. Specifically, we focused on

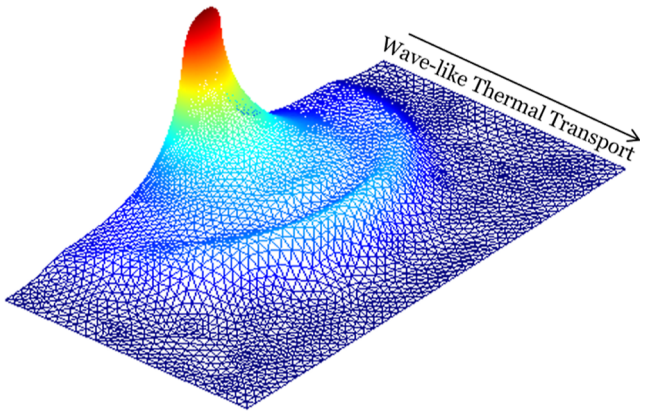


**Figure 12.** Thermal wave-like transport in graphene at $t$ = 1.12 ns for $T_0$ = 80 K using the DPL model.

the heat pulse propagated from the hot spot for phonon engineering applications. The present methodology is capable of predicting the thermal wave-like transport from the hot spot in realistic materials. Figure 13 shows the contour of temperature

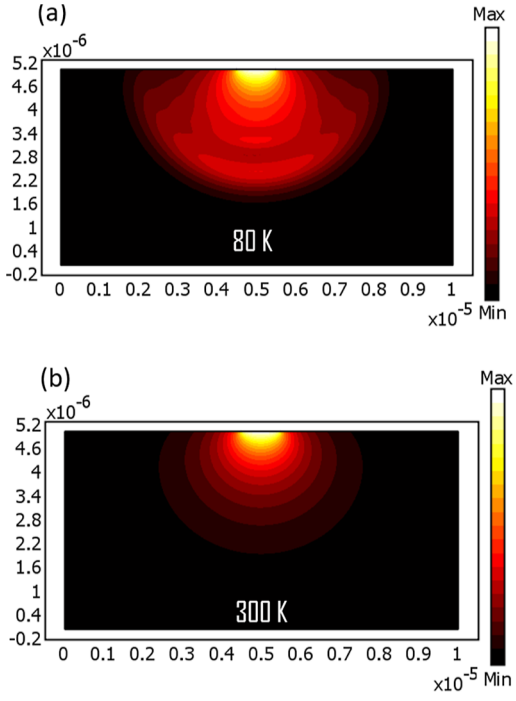


**Figure 13.** Contour plots of temperature distribution in graphene at $t$ = 1 ns using the DPL model for (a) $T_0$ = 80 K and (b) $T_0$ = 300 K.

distribution for (a) $T_0$ = 80 K and (b) $T_0$ = 300 K for a time scale of 1 ns. The applied heat source propagates within the graphene sample in the form of wave-like behavior as shown in Figure 13a. In comparison, in wave-like heat transport, the temperature is oscillating between negative and positive displacement. In the diffusive heat transport, the phonon momentum is destroyed by


https://doi.org/10.1021/acsomega.3c02558
ACS Omega 2023, 8, 23964−23974

significant *R*-scattering without any nonlocalities as shown Figure 13b.

## ■ ASSOCIATED CONTENT

### Data Availability Statement

The data that support the findings of this study are available from the corresponding author upon reasonable request.

### Supporting Information

The Supporting Information is available free of charge at https://pubs.acs.org/doi/10.1021/acsomega.3c02558.

Description of non-Fourier heat transport; derivation of BTJ; and size effects on hydrodynamic heat transport (PDF)

## ■ AUTHOR INFORMATION


### Corresponding Author

**Houssem Rezgui** − *Laboratory of Thermal Processes, Research and Technology Centre of Energy, Hammam Lif 2050, Tunisia; University of Tunis El Manar, Tunis 2092, Tunisia;* orcid.org/0000-0002-9618-7863; Email: houssem.rezgui@fst.utm.tn

Complete contact information is available at: https://pubs.acs.org/10.1021/acsomega.3c02558


### Notes

The author declares no competing financial interest.

## ■ ACKNOWLEDGMENTS

We appreciate Drs. Y. Guo, A. Beardo, C. Zhang, and J. Baker for their helpful remarks and scientific discussions.

## ■ REFERENCES


(1) Wehmeyer, G.; Yabuki, T.; Monachon, C.; Wu, J.; Dames, C. Thermal diodes, regulators, and switches: Physical mechanisms and potential applications. *Appl. Phys. Rev.* **2017**, *4*, 041304.

(2) Fiorino, A.; Thompson, D.; Zhu, L.; Mittapally, R.; Biehs, S. A.; Bezencenet, O.; El-Bondry, N.; Bansropun, S.; Ben-Abdallah, P.; Meyhofer, E.; et al. A thermal diode based on nanoscale thermal radiation. *ACS Nano* **2018**, *12*, 5774−5779.

(3) Cahill, D. G.; Braun, P. V.; Chen, G.; Clarke, D. R.; Fan, S.; Goodson, K. E.; Keblinski, P.; King, W. P.; Mahan, G. D.; Majumdar, A.; et al. Nanoscale thermal transport. II 2003−2012. *Appl. Phys. Rev.* **2014**, *1*, 011305.

(4) Rezgui, H.; Nasri, F.; Ben Aissa, M. F.; Belmabrouk, H.; Guizani, A. A. Modeling Thermal Performance of Nano-GNRFET Transistors Using Ballistic-Diffusive Equation. *IEEE Trans. Electron Devices* **2018**, *65*, 1611−1616.

(5) Schwierz, F.; Pezoldt, J.; Granzner, R. Two-dimensional materials and their prospects in transistor electronics. *Nanoscale* **2015**, *7*, 8261−8283.

(6) Zhang, H.; Wang, H.; Xiong, S.; Han, H.; Volz, S.; Ni, Y. Multi-Scale modeling of heat dissipation in 2D transistors based on phosphorene and silicene. *J. Phys. Chem. C* **2018**, *122*, 2641−2647.

(7) Rezgui, H.; Nasri, F.; Ali, A. B. H.; Guizani, A. A. Analysis of the ultrafast transient heat transport in sub-7-nm SOI FinFETs technology nodes using phonon hydrodynamic equation. *IEEE Trans. Electron Devices* **2021**, *68*, 10−16.

(8) Hu, Y.; Zeng, L.; Minnich, A. J.; Dresselhaus, M. S.; Chen, G. Spectral mapping of thermal conductivity through nanoscale ballistic transport. *Nat. Commun.* **2015**, *10*, 701−706.

(9) Ziabari, A.; Torres, P.; Vermeersch, B.; Xuan, Y.; Cartoixà, X.; Torelló, A.; Bahk, J. H.; Koh, Y. R.; Parsa, M.; Ye, P. D.; Alvarez, F. X.; Shakouri, A. Full-field thermal imaging of quasiballistic crosstalk reduction in nanoscale devices. *Nat. Commun.* **2018**, *9*, 255.

(10) Alajlouni, S.; Beardo, A.; Sendra, L.; Ziabari, A.; Bafaluy, J.; Camacho, J.; Xuan, Y.; Alvarez, F. X.; Shakouri, A. Geometrical quasi-ballistic effects on thermal transport in nanostructured devices. *Nano Res.* **2021**, *14*, 945−952.

(11) Li, X.; Lee, S. Crossover of ballistic, hydrodynamic, and diffusive phonon transport in suspended graphene. *Phys. Rev. B* **2019**, *99*, 085202.

(12) Luo, X.; Guo, Y.; Wang, M.; Yi, H. Direct simulation of second sound in graphene by solving the phonon Boltzmann equation via a multiscale scheme. *Phys. Rev. B* **2019**, *100*, 155401.

(13) Zhang, C.; Guo, Z. A transient heat conduction phenomenon to distinguish the hydrodynamic and (quasi) ballistic phonon transport. *Int. J. Heat Mass Transfer* **2021**, *181*, 121847.

(14) Lee, S.; Broido, D.; Esfarjani, K.; Chen, G. Hydrodynamic phonon transport in suspended graphene. *Nat. Commun.* **2015**, *6*, 6290.

(15) Cepellotti, A.; Fugallo, G.; Paulatto, L.; Lazzeri, M.; Mauri, F.; Marzari, N. Phonon hydrodynamics in two-dimensional materials. *Nat. Commun.* **2015**, *6*, 6400.

(16) Jeong, J.; Li, X.; Lee, S.; Shi, L.; Wang, Y. Transient hydrodynamic lattice cooling by picosecond laser irradiation of graphite. *Phys. Rev. Lett.* **2021**, *127*, 085901.

(17) Ding, Z.; Chen, K.; Song, B.; Shin, J.; Maznev, A. A.; Nelson, K. A.; Chen, G. Observation of second sound in graphite over 200K. *Nat. Commun.* **2022**, *13*, 285.

(18) Guo, Y.; Zhang, Z.; Bescond, M.; Xiong, S.; Wang, M.; Nomura, M.; Volz, S. Size effect on phonon hydrodynamics in graphite microstructures and nanostructures. *Phys. Rev. B* **2021**, *104*, 075450.

(19) Zhang, C.; Huberman, S.; Wu, L. On the emergence of heat wave in the transient thermal grating geometry. *J. Appl. Phys.* **2022**, *132*, 085103.

(20) Guo, Y.; Wang, M. Lattice Boltzmann scheme for hydrodynamic equation of phonon transport. *Int. J. Therm. Sci.* **2022**, *171*, 107178.

(21) Chen, G. Non-Fourier phonon heat conduction at the microscale and nanoscale. *Nat. Rev. Phys.* **2021**, *3*, 555−569.

(22) Ackerman, C. C.; Bertman, B.; Fairbank, H. A.; Guyer, R. A. Second sound in solid helium. *Phys. Rev. Lett.* **1966**, *16*, 789−791.

(23) Markov, M.; Sjakste, J.; Barbarino, G.; Fugallo, G.; Paulatto, L.; Lazzeri, M.; Mauri, F.; Vast, N. Hydrodynamic Heat Transport Regime in Bismuth: A Theoretical Viewpoint. *Phys. Rev. Lett.* **2018**, *120*, 075901.

(24) Jackson, H. E.; Walker, C. T. Thermal conductivity, second sound, and phonon-phonon interactions in NaF. *Phys. Rev. B: Solid State* **1971**, *3*, 1428−1439.

(25) Huberman, S.; Duncan, R. A.; Chen, K.; Song, B.; Chiloyan, V.; Ding, Z.; Maznev, A. A.; Chen, G.; Nelson, K. A. Observation of second sound in graphite at temperatures above 100 K. *Science* **2019**, *364*, 375−379.

(26) Guyer, R. A.; Krumhansl, J. A. Thermal conductivity, second sound, and phonon hydrodynamic phenomena in nonmetallic crystals. *Phys. Rev.* **1966**, *148*, 778.

(27) Guo, H.; Ilseven, E.; Falkovich, G.; Levitov, L. S. Higher-than-ballistic conduction of viscous electron flows. *Proc. Natl. Acad. Sci. U.S.A.* **2017**, *114*, 3068−3073.

(28) Cattaneo, C. A from of heat conduction equation which eliminates the paradox of instantaneous propagation. *C. R. Acad. Sci.* **1958**, *247*, 431.

(29) Vernotte, P. les paradoxes de la théorie continue de l'équation de la chaleur. *C. R. Acad. Sci.* **1958**, *246*, 3154−3155.

(30) Tzou, D. Y. *Macro- to Microscale Heat Transfer: The Lagging Behavior*; Taylor & Francis: Washington, DC, 1997.

(31) Tzou, D. Y. Nonlocal behavior in phonon transport. *Int. J. Heat Mass Transfer* **2011**, *54*, 475−481.

(32) Tzou, D. Y.; Guo, Z. Y. Nonlocal behavior in thermal lagging. *Int. J. Therm. Sci.* **2010**, *49*, 1133−1137.

(33) Guyer, R. A.; Krumhansl, J. A. Solution of the linearized phonon Boltzmann equation. *Phys. Rev.* **1966**, *148*, 766−778.

(34) Guo, Y.; Wang, M. Phonon hydrodynamics for nanoscale heat transport at ordinary temperatures. *Phys. Rev. B* **2018**, *97*, 035421.

(35) Hua, Y. C.; Cao, B. Y. Phonon ballistic-diffusive heat conduction in silicon nanofilms by Monte Carlo simulations. *Int. J. Heat Mass Transfer* **2014**, *78*, 755−759.
(36) Sobolev, S. L. Discrete space-time model for heat conduction: Application to size dependent thermal conductivity in nano-films. *Int. J. Heat Mass Transfer* **2017**, *108*, 933−939.
(37) Hua, Y. C.; Cao, B. Y. Slip Boundary Conditions in ballistic−diffusive heat transport in nanostructures. *Nanoscale Microscale Thermophys. Eng.* **2017**, *21*, 159−176.
(38) Gandolfi, M.; Benetti, G.; Glorieux, C.; Giannetti, C.; Banfi, F. Accessing temperature waves: A dispersion relation perspective. *Int. J. Heat Mass Transfer* **2019**, *143*, 118553.
(39) Mazza, G.; Gandolfi, M.; Capone, M.; Banfi, F.; Giannetti, C. Thermal dynamics and electronic temperature waves in layered correlated materials. *Nat. Commun.* **2021**, *12*, 6904.
(40) Li, C.; Miao, J.; Yang, K.; Guo, X.; Tu, J.; Huang, P.; Zhang, D. Fourier and non-Fourier bio-heat transfer models to predict ex vivo temperature response to focused ultrasound heating. *J. Appl. Phys.* **2018**, *123*, 174906.
(41) Gandolfi, M.; Giannetti, C.; Banfi, F. Temperonic crystal: A superlattice for temperature waves in graphene. *Phys. Rev. Lett.* **2020**, *125*, 265901.
(42) Guo, Y.; Wang, M. Phonon hydrodynamics and its applications in nanoscale heat transport. *Phys. Rep.* **2015**, *595*, 1−44.
(43) Beardo, A.; Lopez-Suarez, M.; Perez, L. A.; Sendra, L.; Alonso, M. I.; Melis, C.; Bafaluy, J.; Camacho, J.; Colombo, L.; Rurali, R.; et al. Observation of second sound in a rapidly varying temperature field in Ge. *Sci. Adv.* **2021**, *7*, No. eabg4677.
(44) Ziman, J. M. *Electron and Phonons: The Theory of Transport Phenomena in Solids*; Clarendon Press: Oxford, London, 2001.
(45) Jiaung, W.-S.; Ho, J.-R. Lattice-Boltzmann modeling of Phonon hydrodynamics. *Phys. Rev. E: Stat., Nonlinear, Soft Matter Phys.* **2008**, *77*, 066710.
(46) Guo, Z.; Xu, K. Discrete unified gas kinetic scheme for multiscale heat transfer based on the phonon Boltzmann transport equation. *Int. J. Heat Mass Transfer* **2016**, *102*, 944−958.
(47) Ding, Z.; Zhou, J.; Song, B.; Chiloyan, V.; Li, M.; Liu, T.; Chen, G. Phonon hydrodynamic heat conduction and Knudsen minimum in graphite. *Nano Lett.* **2018**, *18*, 638−649.
(48) Cercignani, C.; Daneri, A. Flow of a rarefied gas between two parallel plates. *J. Appl. Phys.* **1963**, *34*, 3509−3513.
(49) Ghosh, K.; Kusiak, A.; Battaglia, J. L. Phonon hydrodynamics in crystalline GeTe at low temperature. *Phys. Rev. B* **2020**, *102*, 094311.
(50) McBennett, B.; Beardo, A.; Nelson, E. E.; Abad, B.; Frazer, T. D.; Adak, A.; Esashi, Y.; Li, B.; Kapteyn, H. C.; Murnane, M. M.; et al. Universal behavior of highly confined heat flow in semiconductor nanosystems: From nanomeshes to metalattices. *Nano Lett.* **2023**, *23*, 2129−2136.
(51) Nie, B. D.; Cao, B. Y. Interfacial thermal resistance in phonon hydrodynamic heat conduction. *J. Appl. Phys.* **2022**, *131*, 064302.
(52) Nie, B. D.; Cao, B. Y. Thermal wave in phonon hydrodynamic regime by phonon Monte Carlo simulations. *Nanoscale Microscale Thermophys. Eng.* **2020**, *24*, 94−122.
(53) Hardy, R. J. Phonon Boltzmann equation and second sound in solids. *Phys. Rev. B: Solid State* **1970**, *2*, 1193−1207.
(54) Varshni, Y. P.; Konti, A. Second-sound velocities in cubic crystals. *Phys. Rev. B: Solid State* **1972**, *6*, 1532−1536.
(55) Sendra, L.; Beardo, A.; Bafaluy, J.; Torres, P.; Alvarez, F. X.; Camacho, J. Hydrodynamic heat transport in dielectric crystals in the collective limit and the drifting/driftless velocity conundrum. *Phys. Rev. B* **2022**, *106*, 155301.
(56) Shang, M. Y.; Mao, W. H.; Yang, N.; Li, B.; Lu, J. T. Unified theory of second sound in two-dimensional materials. *Phys. Rev. B* **2022**, *105*, 165423.


https://doi.org/10.1021/acsomega.3c02558
*ACS Omega* 2023, 8, 23964−23974